Defect structures in (001) zincblende GaN/3C-SiC nucleation layers

Petr Vacek[1, 2, a, b], Martin Frentrup[1, b], Lok Yi Lee[1, b], Fabien C.-P. Massabuau[1, 3], Menno J. Kappers[1], David J. Wallis[1, 4], Roman Gröger[2], and Rachel A. Oliver[1]

[1] Department of Materials Science and Metallurgy, University of Cambridge, 27 Charles Babbage Road, Cambridge, CB3 0FS, United Kingdom

[2] Institute of Physics of Materials & CEITEC IPM, Czech Academy of Sciences, Žižkova 22, 61600 Brno, Czech Republic

[3] Department of Physics, SUPA, University of Strathclyde, 107 Rottenrow East, Glasgow, G4 0NG, United Kingdom

[4] Centre for High Frequency Engineering, University of Cardiff, 5 The Parade, Newport Road, Cardiff, CF24 3AA, United Kingdom

[a] Corresponding author: vacek@ipm.cz
[b] P Vacek, M Frentrup and L Y Lee contributed equally to this work.

Abstract

The defect structure of zincblende GaN nucleation layers grown by metalorganic vapor-phase epitaxy on 3C-SiC/Si (001) was investigated by high-resolution scanning transmission electron microscopy. Perfect dislocations, partial dislocations, and stacking faults are present in the layers. Perfect dislocations are identified as 60° mixed-type and act as misfit dislocations to relieve the compressive lattice mismatch strain in GaN. Stacking faults are mainly bounded by 30° Shockley partial dislocations and rarely by Lomer-Cottrell partial dislocations, both of which are able to relieve the compressive lattice mismatch strain in the layer. We propose that the stacking faults and their partial dislocations originate from the dissociation of perfect dislocations present in the zincblende GaN layer, and by direct nucleation of partial dislocations loops from the surface. These are the two main mechanisms, which lead to the final defect structure of the zincblende GaN nucleation layers.

Introduction

Over the past 25 years, wurtzite (wz) III-nitrides have found applications in bright and efficient light sources, mainly blue-wavelength light emitting diodes (LEDs) and laser diodes. However, their efficiency as green-wavelength emitting devices is significantly reduced due to the polarization fields present in quantum wells grown along the commonly used [0001] or *c*-direction. These polarization fields cause a spatial separation of charge carriers, resulting in a reduced radiative recombination efficiency. Cubic, zincblende (zb) III-nitride heterostructures grown along the ⟨001⟩ orientation do not exhibit these polarization fields and are consequently promising materials for efficient green-wavelength emitting devices.[1]

Although the zb phase is metastable, it can be stabilized by epitaxial growth on cubic substrates. As there are no native substrates for zb III-nitride epitaxy, foreign substrates such as GaAs,[2–4] 3C-SiC,[5,6] and micro-structured Si (001)[7] are used instead. In all these cases, the GaN epilayer suffers from a high density of stacking faults (SFs). These SFs often nucleate at the GaN/substrate heterointerface and their density decreases with film thickness by annihilation between SFs on different {111} planes.[8] Zb-GaN may also suffer from the presence of other, more extended defective inclusions, such as bunched SFs and wz-lamellae formed by a change of the stacking sequence of the closed-packed {111} planes, when the growth conditions are not fully optimized to suppress such changes. Individual and bunched SFs may negatively impact the optical properties of the material as was shown by Church *et al.*[9] using photoluminescence spectroscopy, and Kemper *et al.*[10] using cathodoluminescence spectroscopy in a scanning transmission electron microscope. The former suggested that SFs affected the optical emission due to quantum-well like band alignment between the faulted and unfaulted region, whilst the latter suggested that SFs were associated with non-radiative recombination pathways.

The origin of dislocations and SFs in zb-GaN is not well understood and only a few studies so far have been dedicated to it.[2,3,11,12] Brandt, Trampert and their coworkers reported on the defect formation in zb-GaN on GaAs.[2,3] They found that the {111} SFs in zb-GaN are related to a regular array of misfit dislocations, formed to compensate for the lattice mismatch at the heterointerface with GaAs. On the other hand, the works by Lorenz *et al.*[11] and Wei *et al.*[12], on the growth of zb-GaN on sapphire and 3C-SiC substrates respectively, suggest that exposed {111} facets of the zb-GaN NLs may promote the formation of SFs and wz inclusions.

It is clear from the dearth of literature that further investigation is required for a deeper understanding of defect properties and dislocation nucleation mechanisms in heteroepitaxially grown zb-GaN. Because dislocations are known to nucleate in the heteroepitaxial interface region, a model system of thin zb-GaN nucleation layers (NLs) grown on (001) 3C-SiC/Si[13] was chosen for a detailed scanning transmission electron microscopy (STEM) study. To identify the formation mechanisms of dislocations and SFs in zb-GaN, we regard mechanisms that are known from the literature to occur in face-centered cubic materials, as well as mechanisms relevant to defect formation in heteroepitaxial growth of strained thin films more broadly. Hence, we consider a number of standard processes for defect formation, namely the coalescence of nucleation islands,[14,15] the agglomeration of vacancies,[16] the glide of dislocations from the free surface, and the formation and dissociation of strain-relieving dislocations at the film/substrate heterointerface.[17–20] We assess our TEM results against each of these mechanisms and define the likely origins of dislocations and SFs.

Experimental

The investigated samples were the same as those described in Ref.[13] Zb-GaN NLs up to 44 nm thickness were grown by metalorganic vapor-phase epitaxy (MOVPE) in a 6 × 2-inch Thomas Swan close-coupled showerhead reactor using trimethylgallium (TMG) and ammonia (NH_3) as

precursors. A set of as-grown GaN NLs was immediately cooled down to room temperature after growth at 600 ºC, while a second set of annealed NLs underwent an additional thermal treatment to 885 ºC in an atmosphere of NH_3 and H_2 resembling the temperature ramp to start epilayer growth, before cooling. The substrates used for the GaN epitaxy were ~2 cm × 2 cm pieces cleaved from chemically-mechanically polished ~3 μm-thick 3C-SiC layers grown on 6 inch-diameter, 1000 μm-thick Si (001) provided by Anvil Semiconductors Ltd. The Si wafers had either a 4° or 2º miscut towards the [110] in-plane direction to prevent the formation of anti-phase domains in the 3C-SiC and GaN layers.[21]

X-ray diffraction (XRD) measurements have previously revealed that the zb-GaN NLs are (001) oriented and have high phase purity, as shown by the absence of any wz phase reflections.[13] However, the elongation of the zb-GaN reflections towards the ⟨111⟩ directions indicated the presence of {111}-type SFs in the NLs.

As the formation of SFs might be correlated to the presence of pronounced crystal facets, particularly the {111} facets, facet angles of a large number of islands have been measured using atomic force microscopy (AFM) and transmission electron microscopy (TEM).

For the AFM analysis, a Bruker Dimension Icon atomic force microscope was employed in PeakForce Tapping mode, using ScanAsyst-Air-HR probes from Bruker Nano Inc. with a nominal tip radius of 2 nm, a front tip angle of 15° and a back tip angle of 25°. The facet angles of well-separated nucleation islands on particularly thin NL samples were always measured by the front of the AFM tip to avoid tip-related artefacts and accurately measure the facet angles. The island facet angles with respect to the 3C-SiC surface were then analyzed with the free software package Gwyddion[22] by taking line profiles at the facet locations.

To investigate the local distribution of SFs and dislocations present in the NLs, high-resolution scanning transmission electron microscopy (HRSTEM) using a high angle annular dark field detector (HAADF) and high-resolution transmission electron microscopy (HRTEM) were

utilized. Thin cross-sectional specimens for TEM were prepared by mechanical grinding and polishing, followed by Ar^+ ion milling and a final low-voltage ion polish. The foil specimens were oriented such that the zone axis (viewing direction) was along the $[\bar{1}10]$ direction. HRSTEM imaging on these foils was performed by an aberration corrected FEI Titan^3 microscope operating at 300 kV, 25 mrad convergence semi-angle with 5.6 nm estimated depth of focus, and 40-200 mrad HAADF collection angle range. HRTEM imaging was performed by a FEI Tecnai F20 microscope operating at 200 kV. An average background subtraction filter was applied in some cases to remove noise from the STEM images.

To analyze the type and distribution of defects in the STEM images, the software package Digital Micrograph was utilized using a Fast Fourier Transform approach as described by Wen *et al.*[23]

Results and Discussion

(i) Overview of the GaN nucleation layer characteristics

Our previous work in Ref.[13] highlighted the effect of the thickness and anneal treatment on the morphology and surface coverage of zb-GaN NLs grown on 3C-SiC/Si substrates. This paper focuses on the defect structure of four samples of the same series, namely the nominally 3 nm- and 22 nm-thick as-grown and annealed NL samples. The variation in surface morphology of these zb-GaN NLs is shown in the 500 nm × 500 nm AFM height scans in Figure 1. It is clear from Figure 1 (a) and (b), that both as-grown NLs consist of coalesced islands, which are elongated along the $[\bar{1}10]$ direction, perpendicular to the miscut direction. The AFM scans also show that for the 22 nm-thick NL the surface features become slightly larger in both in-plane directions compared with the 3 nm-thick NL, while the substrate coverage becomes nearly complete. The effect of the high temperature anneal treatment in H_2/NH_3 is presented in Figure 1 (c) and (d), which show that the surface morphology of the annealed NLs also consists of

features elongated in the $[\bar{1}10]$ direction as was observed in Figure 1 (a) and (b) for the as-grown NLs. The annealed sample with a nominal thickness of 3 nm shows areas of exposed 3C-SiC substrate and individual GaN nuclei, whereas the GaN nuclei in the 22nm-thick annealed sample form a more continuous zb-GaN layer and cover the substrate completely. Desorption of GaN takes place during the anneal treatment in both samples, but the total material loss is larger for the thinnest NL, possibly due to the larger surface area provided for material desorption to occur.[13]

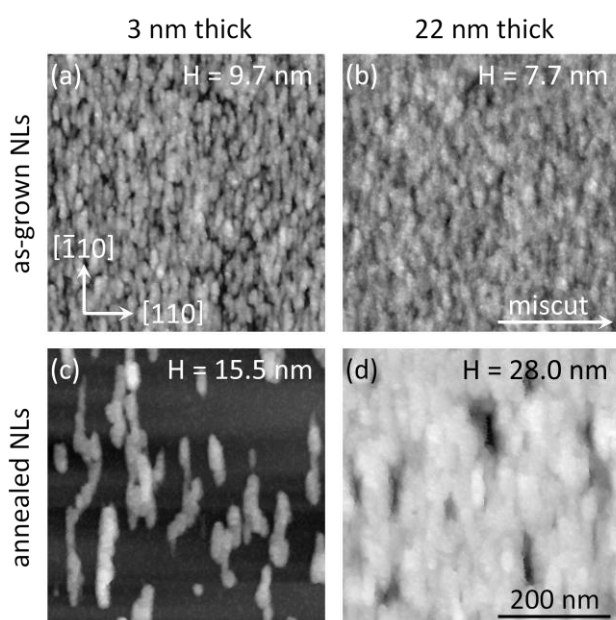

Figure 1: AFM height scans of the nominally 3 nm- and 22 nm-thick zb-GaN NLs grown on 3C-SiC with 4°-miscut, showing the surface morphology before (a, b) and after (c, d) the thermal anneal treatment in H_2/NH_3. The height ranges from black to white (H) are stated in each AFM image.

In Figure 2 (a) and (b), we show cross-sectional HRSTEM and HRTEM images of the nominally 3 nm-thick as-grown and annealed GaN samples respectively. The 3C-SiC template surface appears atomically smooth with steps of height of one monolayer at regular intervals due to the miscut of the substrate. Two {111} SFs can be observed in the 3C-SiC epilayer terminating at the surface in Figure 2 (b). Interestingly, the GaN islands showed no clear

preference for the nucleation on surface steps or on sites where SFs from the 3C-SiC layer terminate at the GaN/3C-SiC interface. Occasionally, we observe in STEM hexagonal patterns of contrast within the NLs as highlighted by yellow and green dots in the inset of Figure 2 (a). These signify SFs in the [110] zone perpendicular to the view direction, as we will discuss more in detail in the supplementary material. TEM images taken along the [110] zone axis (not shown) revealed no significant difference in the defect structure compared to the TEM images presented here for the [$\bar{1}$10] zone axis other than the lack of interfacial steps as the sample miscut has no effect for this view direction.

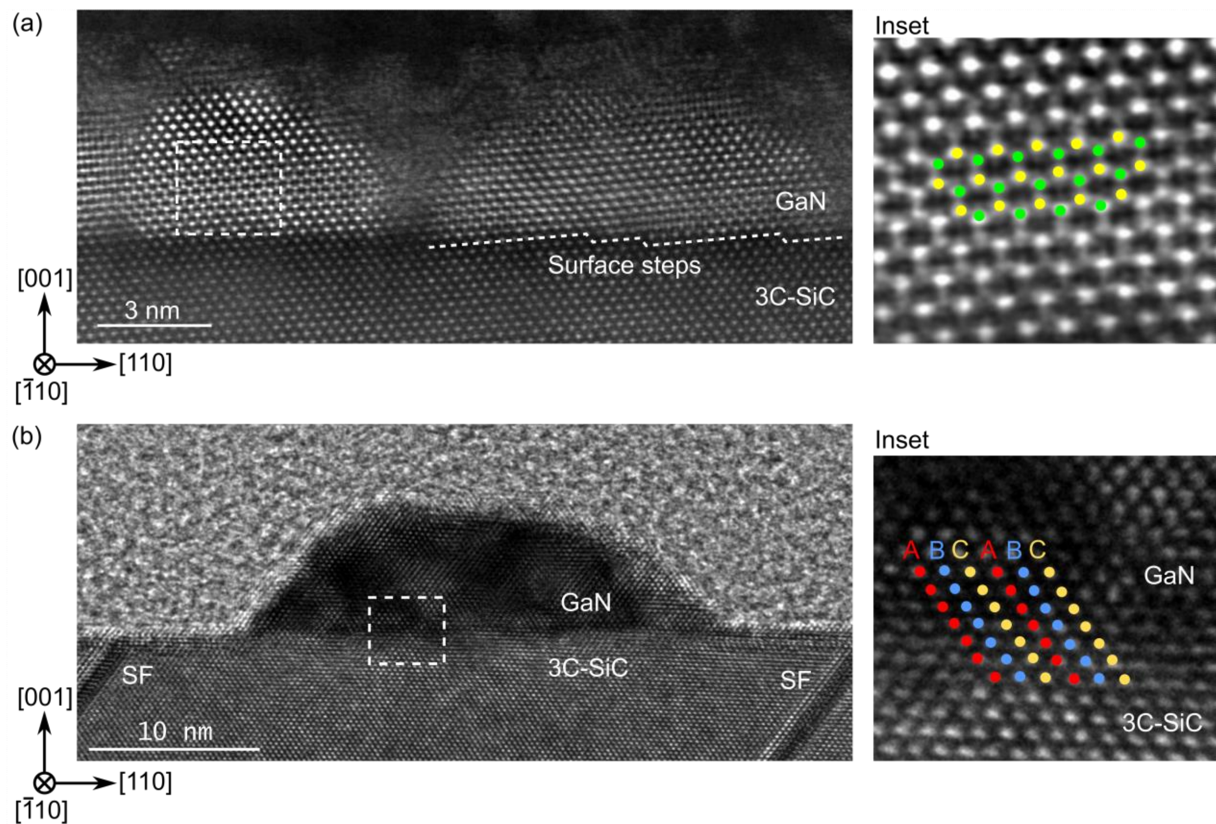

Figure 2: Cross-sectional HRSTEM image of the nominally 3 nm-thick as-grown zb-GaN NL (a), with a hexagonal pattern highlighted by green and yellow dots in the inset. Cross-sectional HRTEM image of an annealed zb-GaN island, with SFs clearly visible in the 3C-SiC substrate (b), and characteristic ABCABC stacking shown in the inset.

The TEM images in Figure 2 reveal that the GaN islands grow epitaxially in the zb phase and (001) orientation on the 3C-SiC surface, with no observable amorphous layer at the interface. This is evident from the characteristic ABCABC stacking of the {111} bi-layers in zb-GaN, which is maintained from the 3C-SiC substrate as highlighted in the inset of (b). The epitaxial relationship is not only observed for individual islands in the thinnest samples, but also for all other samples investigated in this study. The absence of an amorphous interlayer confirms that the thermal nitridation step preceding the NL growth[13] provides a clean substrate surface for GaN growth, which is in contrast to an earlier report by Paisley et al.[24] on the presence of an amorphous interlayer between GaN and 3C-SiC. Furthermore, the TEM images in Figure 2 show no shift at the interface between the patterns of Ga atoms in zb-GaN and Si atoms in 3C-SiC, which implies that Ga atoms occupy Si-sites and N atoms occupy C-sites in the zb structure. This is in agreement with atom radii ($r_C < r_{Si}$, $r_N < r_{Ga}$) and polarity ($EN_C > EN_{Si}$, $EN_N > EN_{Ga}$) considerations, suggesting that zb-GaN is attached to 3C-SiC either via Si-N bonds or C-Ga bonds. Of those, strong Si-N bonds at the interface are likely to be the most common, as (001) 3C-SiC surfaces are usually Si-terminated.[25] However, some intermixing with Ga-C bonds at the interface must exist in order to maintain charge balance, as illustrated in the sketch in Figure 3. Moreover, it was reported in Refs.[11,26] that the phase and orientation of as-grown wz-GaN NLs on (0001) sapphire change significantly upon thermal annealing. But, no phase transformation from zb to wz was observed in our annealed samples; possibly due to the relatively low anneal temperature of 885°C. Nevertheless, the AFM data in Figure 1 confirm that there is some loss of material and a general increase in island size after the anneal treatment. It has been discussed in various literature reports,[11,12] that exposed {111} facets in zb-GaN layers may promote the formation of SFs or wz inclusions. To study the facets in our NLs at the early stage of growth, we have investigated the nominally 3 nm-thick annealed GaN NL sample in more detail. Its individual well-separated islands, in contrast to the more densely

packed islands of the other samples in this study, allow us to measure island facet angles accurately by removing issues with dense island arrays such as poor tip penetration between islands during AFM measurements and the overlap of islands in projection for TEM analysis. This should provide some insight into which facets are stable under the relevant growth conditions. However, we note that the optimized NL should have complete coverage for the GaN epilayer growth, as gaps in the NL lead to an increased fraction of the wz phase, as shown previously.[13]

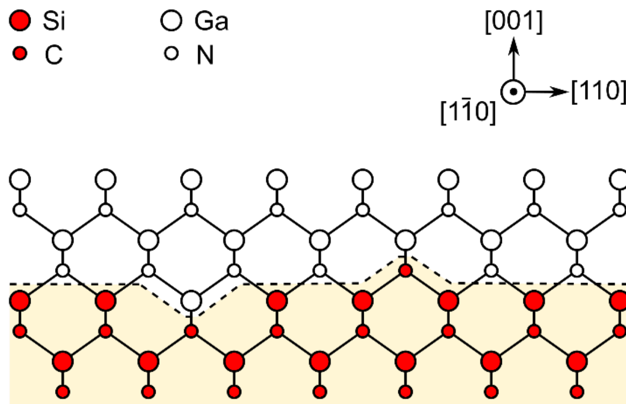

Figure 3: Possible bonding configuration at the interface between zb-GaN and (001) 3C-SiC.

For a large number of islands (> 40), we have analyzed AFM linescans taken parallel to the [110] direction (along the short axis of the islands), which illustrate the low aspect ratio of the islands and facilitate the measurement of side facet angles. To avoid artefacts related to the AFM probe, the island facets were always approached by the front side of the AFM tip, which is inclined away from the surface horizontal by the greater angle. To measure both facets of the individual islands with the same optimally inclined facet of the tip, the sample was rotated by 180° as indicated by the schematics in the insets of Figure 4. As shown by the distribution of island facet angles in Figure 4, no significant difference has been observed between measurements taken by approaching the AFM tip from the [110] (a, front facet) and [$\bar{1}\bar{1}$0] (b,

back facet) directions, except for a small shift along the ordinate, which is caused by the 2° miscut of the substrate. There is a wide range of facet angles between 30° and 65° with respect to the surrounding 3C-SiC surface, and the possible low-index facets within this angular range include {111}, {112}, and {335}, which corresponds to facet angles of 54.7°, 35.3°, and 40.3°, respectively. Such facets have also been observed by HRTEM and HRSTEM for 29 isolated islands studied by electron microscopy, such as in Figure 2 (b). This suggests that {111} facets are possible under the conditions used for the NL growth and annealing and hence, even in the films with more tightly packed islands, they may be available to act as initiation points for the formation of SFs or wz inclusions,[11,12] and therefore should be suppressed or avoided altogether. However, the proportion and size of low-index facets in our GaN NL samples is small, but may be a concern when acting as nucleation sites of wz inclusions during the subsequent high-temperature epilayer growth.

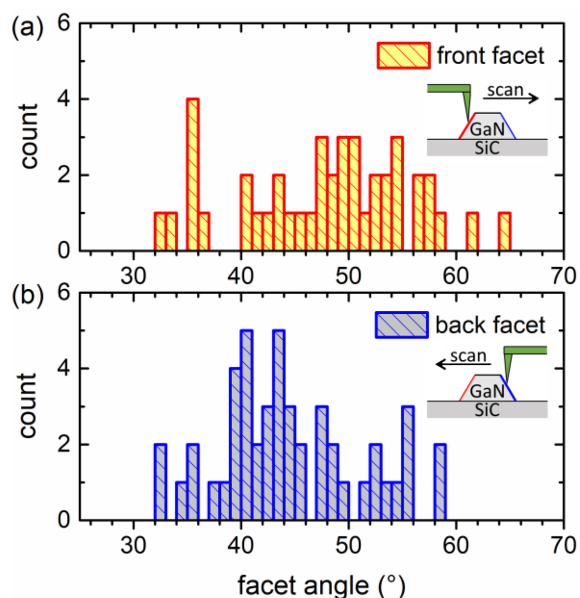

Figure 4: Distribution of facet angles with respect to the surrounding surface of a nominally 3 nm-thick annealed zb-GaN NL measured by approaching the AFM tip from the [110] (a, front facet) and $[\bar{1}\bar{1}0]$ (b, back facet) directions.

The heteroepitaxially-grown NL samples studied here exhibit a rich microstructure, containing perfect and partial dislocations, as well as SFs. Across the available data, we have no evidence for a regular array of these perfect and partial misfit dislocations at the interface between 3C-SiC and zb-GaN. Instead, the misfit dislocations are found to be randomly distributed along the interface for all samples in this study. This is in contrast to reports from Brandt *et al.*, who observed a coincidence lattice with a regular array of misfit dislocations occurring at every 5 {111} planes of zb-GaN on GaAs (001), formed to accommodate the lattice mismatch.[2,3] The difference in the defect distribution can be explained by the different lattice mismatch between the two heterosystems, which is -20.3% for zb-GaN/GaAs (001) compared to only +3.4% for zb-GaN/3C-SiC (001).[27] In the former case, the lattice mismatch is too large to nucleate a GaN layer without misfit dislocations, and hence a short-range coincidence lattice initially forms during growth. However, for smaller lattice mismatches, as it is the case for zb-GaN on 3C-SiC (001), a strained NL can initially form with a lower energy than the relaxed structure. Crystal defects, which then nucleate later in the growth process following an increase in strain energy with increasing layer thickness, will form a less regular pattern. Therefore, mechanisms for strain relief other than the formation of a coincidence lattice occur in the zb-GaN/3C-SiC system.

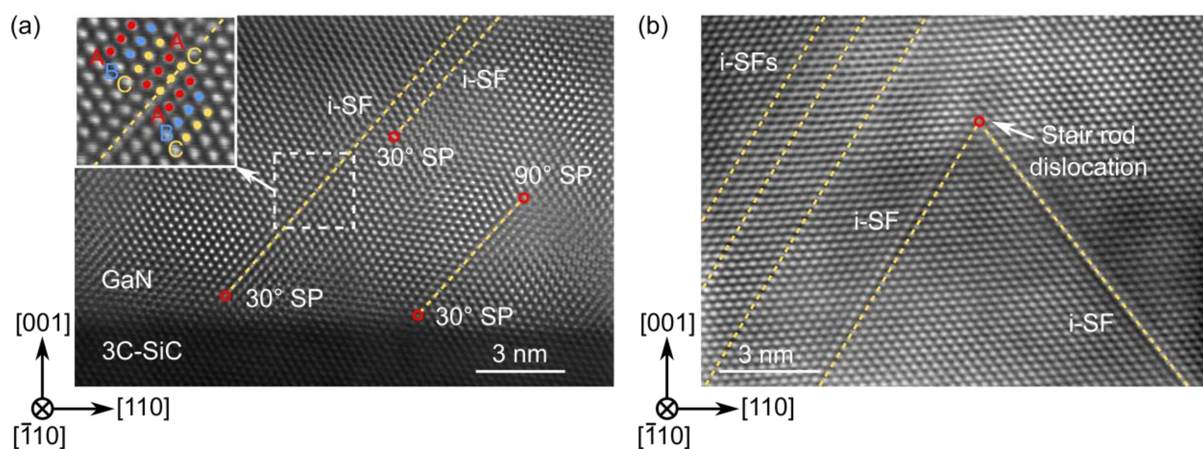

Figure 5: Cross-sectional HRSTEM images of the zb-GaN/3C-SiC (001) interface of a 22 nm-thick as-grown (a) and annealed (b) NL. Shockley partial dislocations (SP) are highlighted by red circles and intrinsic stacking faults (i-SF) by yellow dashed lines, while the stacking sequence of an intrinsic SF is highlighted in the inset of (a). Annihilation of two intrinsic SFs through the formation of a stair-rod partial dislocation (b).

The majority of the planar {111} SFs in the GaN NLs originate at or near the heterointerface with 3C-SiC. They are predominantly of intrinsic type as illustrated in Figure 5 (a) by the missing {111} plane in the stacking sequence ABC**AC**ABC. These i-SFs propagate through the epilayer until they either reach the free surface or annihilate with other SFs. Figure 5 (b) shows such a reaction, by which a stair-rod partial dislocation is formed at the intersection line of two i-SFs. The Burgers vector of this stair-rod partial dislocation is the combination of the Burgers vectors from one Shockley partial dislocation terminating each SF. As the SFs annihilate during the film growth, their density reduces with increasing film thickness.[28]

Occasionally, extrinsic SFs (e-SF) with ABC**B**ABC stacking sequence as shown in Figure 6 were observed in our samples. These e-SFs originate from the 3C-SiC layer and continue into the GaN layer. However, they represent only a small minority of the total SF population in the GaN NL.

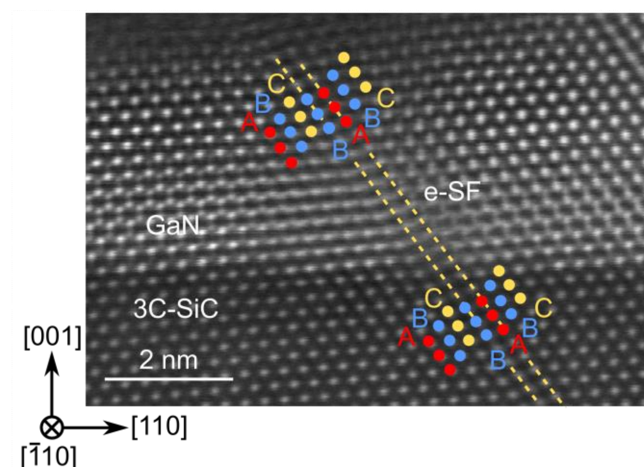

Figure 6: Continuation of an extrinsic stacking fault (e-SF) from the 3C-SiC layer into the zb-GaN NL.

In summarizing section (i), it is established that the low-temperature NLs consist of zb-GaN islands with an epitaxial relationship to the clean 3C-SiC (001) surface. There is no evidence that substrate surface steps function as island nucleation sites. The thermal anneal process reveals an optimal NL thickness marking the complete surface coverage of the substrate by densely-packed GaN islands. The observed perfect and partial dislocations in the zb-GaN are found to be randomly distributed. Intrinsic SFs start at or near the GaN/3C-SiC interface, while a small number of extrinsic SFs penetrate into the GaN layer from the 3C-SiC substrate.

(ii) Defect characteristics & formation mechanisms

The defect characteristics in the zb-GaN NL samples will now be discussed in greater depth, based on the analysis of the relevant TEM images. In addition to discussing the {111} intrinsic SFs, we will consider in more detail the role of partial and perfect misfit dislocations. Since the majority of the SFs originate at or near the GaN/3C-SiC heterointerface, a number of potential SF nucleation processes may be relevant such as island coalescence, agglomeration of vacancies, dissociation of perfect dislocations, and glide of dislocation half-loops from the free surface. These four different likely candidates for a SF formation mechanism will be discussed in the following subsections.

SF formation by island coalescence

It has been proposed by Nix *et al.*[14] and Sheldon *et al.*[15] that during the island coalescence process, neighboring nuclei snap together elastically resulting in a boundary at which a single atomic plane is missing. This would allow the relaxation of a positive lattice mismatch by creating a misfit dislocation at the heterointerface and a SF at the island coalescence boundary, as illustrated schematically in Figure 7 (a). However, this model is only partially supported by

our experimental results. Figure 7 (b) shows a typical cross-sectional HRSTEM HAADF image of coalesced zb-GaN islands grown on the (001) 3C-SiC template. The white dashed line indicates the surface contour of the islands, while the small white arrows mark the likely position of their coalescence boundaries. These apparent island coalescence boundaries are not associated with SFs in the same crystallographic zone in this particular example. The only visible SF in the same zone as the boundary is the extrinsic SF marked by yellow dashed lines, which continues from 3C-SiC to zb-GaN and thus is not related to the island coalescence. From the analysis of a large number of TEM images, we have no evidence that SFs formed in the zb-GaN NLs are regularly located at apparent island coalescence boundaries, identified from the contour of the layer viewed in this zone axis. The light blue ovals in Figure 7 (b) also shows three face-on viewed SFs in the [110] zone, i.e., perpendicular to the view direction of the TEM image (see supplementary material), but, obviously, their association with a coalescence boundary in the [110] zone cannot be examined. Similar face-on viewed SFs were observed within non-coalesced, individual islands, as was shown in Figure 2 (a). These collective observations suggest that different mechanisms other than island coalescence are prevalent during the formation of SFs in the zb-GaN NL at the 3C-SiC heterointerface. One possibility is the formation of SFs by vacancy agglomeration, which is discussed next.

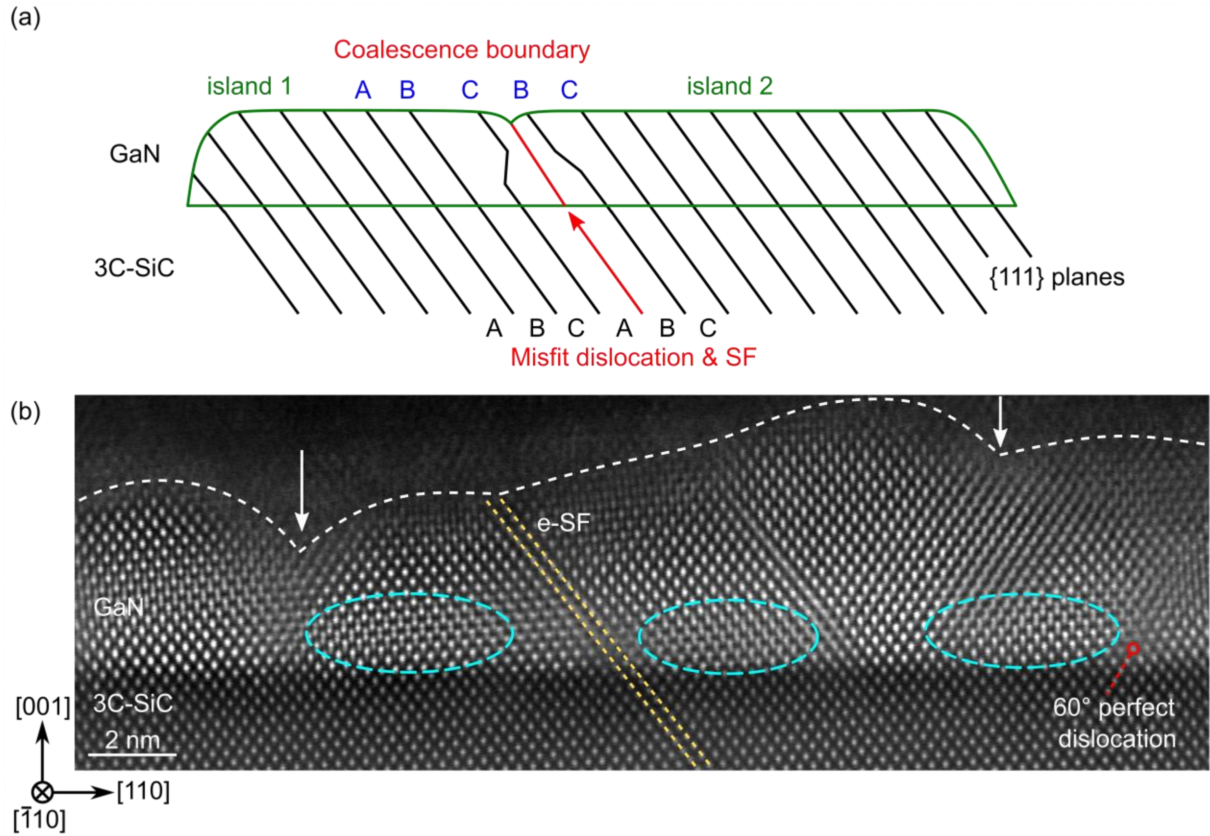

Figure 7: Illustration of the SF formation at the coalescence boundary of two islands (a) and cross-sectional HRSTEM image of the [$\bar{1}$10] zone of a zb-GaN NL grown on 3C-SiC (b). An extrinsic SF (e-SF) in the same zone is highlighted by yellow dashed line, while SFs of the [110] zone normal to the view direction are highlighted in light blue. A 60° perfect misfit dislocation in the right corner is marked in red, and the white arrows indicate the possible location of the coalescence boundaries.

SF formation by vacancy agglomeration

In their work on wz-GaN, Narayanan *et al.*[16] proposed that SFs are formed by diffusion of vacancies to a certain close-packed plane during thermal annealing, which creates a discontinuity in stacking and consequently a SF. A similar process could occur for the {111} planes in zb-GaN, as the low-temperature NL growth conditions here are similar to those typically used for wz-GaN. In zb-GaN this particular SF formation mechanism would result in an intrinsic SF bounded by $\frac{1}{3}\{111\}$ Frank partial dislocations. Although these dislocations are immobile and cannot glide, once such a SF is formed and terminates at the free GaN surface it

would extend as the film grows. However, the absence of Frank partial dislocations in our NL samples means that we have no evidence for the involvement of the condensation of vacancies in the formation of SFs in the zb heterosystem investigated here. Our data thus suggest that this mechanism is unlikely to be of great importance.

SF formation by dissociation of perfect misfit dislocations

A detailed analysis of the defect structure in the zb-GaN NLs revealed that most of the SFs originating at the GaN/3C-SiC heterointerface are bounded by 30° Shockley partial dislocations with Burgers vector $\frac{1}{6}\langle 112\rangle$ as highlighted by the red circles in Figure 5 (a). These partial dislocations might be formed by dissociation of 60° perfect misfit dislocations. In this process, the 30° Shockley partial dislocation remains at the interface and a 90° Shockley partial dislocation is repelled away from it into the layer by Peach-Koehler forces. This dissociation is beneficial to lower the energy in the epilayer and can also occur in stress-free crystals. However, the presence of misfit stresses can influence the distance of the repulsion from the 30° Shockley partial dislocation to allow further reduction of the misfit strain as will be discussed in section iii. In addition to the bounding by 30° Shockley partial dislocation, SFs in zb-GaN are also sporadically bounded by stair-rod partial dislocations, which will be discussed further below.

Not all intrinsic {111}-type SFs extend from these interfacial dislocations to the free GaN surface or annihilate with other SFs within the GaN layer; Figure 5 (a) shows an example where a SF terminates a few nanometers away from the GaN/3C-SiC interface. This particular SF is bounded by a 30° Shockley partial dislocation at the interface and a 90° Shockley partial dislocation at the far end. Overall, this arrangement corresponds to an extended 60° perfect dislocation. Non-dissociated perfect misfit dislocations, as shown in Figure 7, are quite rare and were only observed at the heterointerface. They have been identified as 60° mixed type dislocations with Burgers vector $\frac{1}{2}\langle 101\rangle$.

SFs arranged in Lomer-Cottrell junctions at the interface

As mentioned above, in some rare cases intrinsic SFs are bounded by a stair-rod partial dislocation at step edges of the GaN/3C-SiC heterointerface. An example of this so-called Lomer-Cottrell lock is shown in Figure 8, in which two intrinsic SFs (i-SF1 and i-SF2) extend in a characteristic “V”-shape from such a stair-rod partial dislocation into the layer. In this arrangement, the stair-rod partial dislocation is immobile and has a pure edge character. The Burgers vector of the stair-rod partial dislocation in Figure 8 is $\frac{1}{6}[\bar{1}\bar{1}0]$, which is one possible outcome of the reaction of two 30° Shockley partials (e.g. $\frac{1}{6}[\bar{2}11]$ and $\frac{1}{6}[1\bar{2}\bar{1}]$) when two SFs on different {111} planes join. This reaction is energetically favorable according to Frank’s rule and is common in face-centered cubic, diamond cubic, and zb materials.[18,29–31] However, the fact that the two SFs meet exactly at the interface gives this mechanism a low probability. The other scenario is that the stair-rod partial dislocation first nucleated at the heterointerface as a misfit dislocation with the intrinsic SFs extending from it into the GaN layer. This is a reasonable assumption as the critical thickness of the zb-GaN NL is only a few monolayers; as otherwise, the amount of material required to move would be too large.

Alternatively, Lomer-Cottrell junctions at the interface can form by a reaction between dislocations; for example, when an intrinsic SF bounded by a 30° Shockley partial dislocation at the heterointerface transforms into a stair-rod dislocation with Burgers vector $\frac{1}{6}[\bar{1}\bar{1}0]$ and a second intrinsic SF terminated by Shockley partial dislocation, e.g. with Burgers vector $\frac{1}{6}[\bar{1}21]$. The newly formed Shockley partial dislocation could then glide into the layer and extend its associated intrinsic SF to the free GaN surface, forming the arrangement shown in Figure 8. However, considering the magnitude of the Burgers vectors involved in this reaction, the transformation $\frac{1}{6}[\bar{2}11] \rightarrow \frac{1}{6}[\bar{1}\bar{1}0] + \frac{1}{6}[\bar{1}21]$ would be unfavorable according to Frank’s rule

within a zb-GaN layer. However, the fact that all observed stair-rod partial dislocations were located next to a 3C-SiC step edge may suggest that this type of defect arrangement is geometrically driven by such interfacial features.

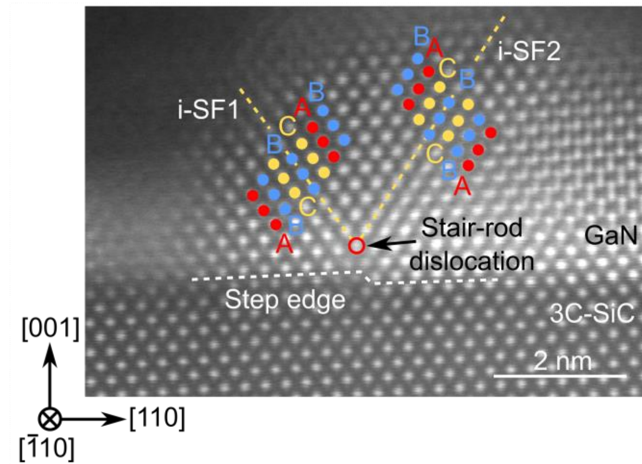

Figure 8: HRSTEM image in cross-sectional view of SFs (i-SF1 and i-SF2) extending from a stair-rod partial dislocation (red circle) located at a step edge of the 3C-SiC/GaN heterointerface. The SFs are intrinsic as indicated by the missing plane in the stacking sequence.

SFs formed by glide from the free surface

Not all {111}-type SFs start directly at the GaN/3C-SiC heterointerface. This is for example the case in Figure 5 (a), where a SF terminated by a 30° Shockley partial dislocation in the GaN layer starts at about 5 nm from the interface. These SFs are possibly formed either by nucleation of partial dislocations as a result of the continuous relaxation of the NL with increasing film thickness, or by glide of partial dislocation half-loops from the free surface into the layer. As the NL is still slightly strained after the first few nanometers,[13] it is impossible to distinguish between the two mechanisms in this particular example. However, it is worth noting that we observe dislocation glide from the free surface in strain-free thick zb-GaN layers, which are currently under investigation as part of our on-going studies.

(iii) Strain relief by defect formation

The discussion above has made it clear that some non-dissociated 60° mixed type perfect misfit dislocations exist at the interface, but many have dissociated into intrinsic SFs bounded by Shockley partial dislocations and a few were bounded by Lomer-Cottrell partial dislocations.

In general, perfect and partial dislocations both contribute to the lattice mismatch strain relief by the edge component of their Burgers vector which lies parallel to the (001) interface. In theory, of those crystal defects observed in our samples most of the lattice mismatch strain at the interface can be compensated by the formation of 60° mixed-type perfect dislocations. For these the edge component of their Burgers vector in $\langle 110 \rangle$ direction normal to the dislocation line is $\frac{a}{2\sqrt{2}}$ (where *a* is the lattice constant of zb-GaN).[17] Compared to this, the projections of the Burgers vector edge components along the $\langle 110 \rangle$ in-plane direction of 30° Shockley partial and 90° Shockley partial dislocations as well as Lomer-Cottrell stair-rod partial dislocations are significantly smaller, namely $\frac{a}{6\sqrt{2}}$, $\frac{a}{3\sqrt{2}}$ and $\frac{a}{3\sqrt{2}}$ respectively.[17] However, as partial dislocations have a shorter Burgers vector than perfect dislocations their formation energy $E \propto G \times b^2$ is significantly lower according to Frank's rule. Therefore, the formation of partial dislocation half-loops at the free surface could be energetically preferable to the nucleation (and dissociation) of perfect dislocations at the interface. This is also expressed in the much lower critical thickness up to which zb-GaN can exist before dislocations are formed. Based on conventional models for closed thin films[32,33] – a condition which is not fully met by 3D zb-GaN NL islands observed in our study – the critical thickness at which 30° SP dislocations start to form is only about half the critical thickness for 60° perfect dislocations.

Furthermore, the type of strain accommodated depends strongly on the defect type and arrangement. Depending on the position of the extra {111} half-plane, 60° perfect dislocations relieve either compressive or tensile in-plane strain in the zb-GaN layer. Similarly, Lomer-

Cottrell dislocations can relieve both types of in-plane strain, depending on the direction of their Burgers vector. However, 30° Shockley partial dislocations located at the interface relieve compressive strain only, while 90° Shockley partial dislocations relieve tensile strain only.[18,19] Note that this is in general true only if the Shockley partials (30° or 90° type) are located at the interface. But, if they are part of a dissociated extended 60° perfect dislocation and terminate within the zb-GaN layer, then the second Shockley partial dislocation at the other end of the SF (90° or 30° type) relieves the same type of strain (compressive or tensile) as the partial dislocation at the interface. Thus, both Shockley partial dislocations compensate the same amount of lattice mismatch strain as a 60° perfect dislocation and their separation lead to a gradual relaxation with increasing film thickness.

As the thin zb-GaN NLs have a slightly larger lattice constant than the 3C-SiC substrate and thus are subjected to compressive strain at the common (001) heterointerface, it is expected that the interface region in GaN shows dislocations which relieve compressive in-plane strain as our TEM experiments confirm. Of the dislocations mentioned above, 90° Shockley partial dislocations were the only ones not observed directly at the interface, but rather at the other end of a dissociated perfect misfit dislocation. The average spacing between the randomly distributed 30° Shockley partial dislocations in the interface was measured to be 5.71 nm (or about 18 {111} planes of zb-GaN), which allows for compensation of about 30% of the lattice mismatch strain. This is in agreement with XRD strain measurements on the samples investigated here, showing a reduction of the 3.4% lattice mismatch strain to about 2.0% within the first 3 nm of growth.[13] Dislocations formed at some distance from the interface then lead to a further gradual relaxation of the misfit strain with increasing layer thickness, as evidenced by the gradual decrease of the compressive in-plane strain with layer thickness.

Covering the main points from the discussion so far, two mechanisms for the formation of intrinsic SFs in zb-GaN NLs on 3C-SiC (001) are proposed. One possible mechanism is the

nucleation of a perfect dislocation at the interface, which dissociates into two partial dislocations bounding the intrinsic SF.[29] This process is energetically beneficial and can lead in some cases to a larger strain release than a non-dissociated perfect dislocation can achieve. For example, a pure screw dislocation at the heterointerface does not accommodate mismatch strain. But, if it dissociates into two 30° Shockley partial dislocations, one of which glides to the free GaN surface and annihilates on the surface, the remaining partial dislocation at the interface relieves lattice mismatch strain.

A second possible mechanism for the formation of SFs in zb-GaN is via the nucleation of partial dislocation half-loops.[19,20] These would form at the surface and glide through the zb-GaN layer on {111} planes (potentially) to the GaN/3C-SiC interface. Also, a partial dislocation with non-zero edge component of the Burgers vector located at the interface allows accommodation of the lattice mismatch strain.

The negative SF energy in zb-GaN[34,35] makes it favorable to extend existing SFs and increase the dimension of dislocation loops. Therefore, SFs rarely terminate at a Shockley partial dislocation within the layer and instead prefer to extend towards the free surface to lower the total energy of the system.

Summary

The defect structure of the zb-GaN layers grown on 3C-SiC/Si (001) was investigated and the possible origin of the observed defects was discussed. Facet angles present in the islands prior to the coalescence were measured by the AFM and some corresponded to short {111} facets, which might induce SF nucleation. Defects present in the layers included perfect dislocations, partial dislocations and predominantly intrinsic stacking faults. The perfect dislocations were 60° mixed-type and acted as misfit dislocations relieving the compressive lattice mismatch strain. No regular arrangement of the misfit dislocations was found at the zb-GaN/3C-SiC

interface of our samples, which is in contrast to reports about zb-GaN layers grown on GaAs. The difference can be explained by the very different lattice mismatch in both heterosystems, which is significantly lower for the use of 3C-SiC templates. The partial dislocations at the interface bounding {111}-type SFs were identified as 30° Shockley partials or sessile Lomer-Cottrell partial dislocations, while in some cases 90° Shockley partial dislocations terminate SFs within the zb-GaN layer as part of an extended perfect dislocation from the interface. The 30° Shockley partials are able to relieve the compressive lattice mismatch strain and their contribution cannot be neglected even though the amount of the strain relieved is only a 1/3 of the strain relief of a 60° mixed-type perfect dislocation. Lomer-Cottrell partial dislocations, which act as misfit dislocations, were found next to SiC step edges in the GaN/3C-SiC interface. We speculate that they are not the outcome of the dislocation reactions of partial dislocations gliding from the surface, but instead that they nucleated from misfit dislocations already present at the interface and that they are possibly initiated by the step-edges.

Based on our findings we propose that partial dislocations and intrinsic SFs either originate from the dissociation of perfect dislocations at the interface or that they directly form at the free surface as a partial dislocation half-loop. We conclude that both mechanisms are taking place in zb-GaN layers. This highlights the importance of controlling the nucleation conditions for zb-GaN growth on 3C-SiC, to reduce the defect formation in the NLs, and consequently in the following zb-GaN thin films.

Supplementary Material

See supplementary material for a detailed analysis of the hexagonal patterns observed in some TEM images of zb-GaN studied in this article.

Acknowledgements

We would like to thank Innovate UK for the financial support within the Energy Catalyst Round 4 - Mid Stage Feasibility scheme (Ref. 102766), and EPSRC for support through grant no. EP/M010589/1 and grant no. EP/R01146X/1. P Vacek would like to thank the Ministry of Education, Youth and Sports of the Czech Republic (MEYS CR) for supporting a 6-month research stay at the Cambridge Centre for Gallium Nitride through the project no. CZ.02.2.69/0.0/0.0/16_027/0008056. The CzechNanoLab project LM2018110 funded by the MEYS CR is gratefully acknowledged for the financial support of the measurements at CEITEC Nano Research Infrastructure. DJ Wallis would like to acknowledge support from EPSRC Manufacturing fellowship, EP/N01202X/2.

Data availability

Datasets that support the findings of this study are openly available from the University of Cambridge research repository at https://doi.org/10.17863/CAM.59167 and from the corresponding author upon request.

References

[1] D.R. Elsaesser, M.T. Durniak, A.S. Bross, and C. Wetzel, J Appl Phys **122**, 115703 (2017).

[2] O. Brandt, H. Yang, A. Trampert, and K. H. Ploog, MRS Proc **395**, 27 (1995).

[3] A. Trampert, O. Brandt, H. Yang, and K.H. Ploog, Appl Phys Lett **70**, 583 (1997).

[4] D. Chandrasekhar, D.J. Smith, S. Strite, M.E. Lin, and H. Morkoç, J Cryst Growth **152**, 135 (1995).

[5] D.J. As, R. Kemper, C. Mietze, T. Wecker, J.K.N. Lindner, P. Veit, A. Dempewolf, F. Bertram, and J. Christen, MRS Proc **1736**, 25 (2014).

[6] E. Martinez-Guerrero, E. Bellet-Amalric, L. Martinet, G. Feuillet, B. Daudin, H. Mariette, P. Holliger, C. Dubois, C. Bru-Chevallier, P. Aboughe Nze, T. Chassagne, G. Ferro, and Y. Monteil, J Appl Phys **91**, 4983 (2002).

[7] C.J.M. Stark, T. Detchprohm, S.C. Lee, Y.-B. Jiang, S.R.J. Brueck, and C. Wetzel, Appl Phys Lett **103**, 232107 (2013).

[8] S. Ruvimov, Z. Liliental-Weber, J. Washburn, T.J. Drummond, M. Hafich, and S.R. Lee, Appl Phys Lett **71**, 2931 (1997).

[9] S.A. Church, S. Hammersley, P.W. Mitchell, M.J. Kappers, S.L. Sahonta, M. Frentrup, D. Nilsson, P.J. Ward, L.J. Shaw, D.J. Wallis, C.J. Humphreys, R.A. Oliver, D.J. Binks, and P. Dawson, Phys Status Solidi B **254**, 1600733 (2017).

[10] R.M. Kemper, P. Veit, C. Mietze, A. Dempewolf, T. Wecker, F. Bertram, J. Christen, J.K.N. Lindner, and D.J. As, Phys Status Solidi C **12**, 469 (2015).

[11] K. Lorenz, M. Gonsalves, W. Kim, V. Narayanan, and S. Mahajan, Appl Phys Lett **77**, 3391 (2000).

[12] C.H. Wei, Z.Y. Xie, L.Y. Li, Q.M. Yu, and J.H. Edgar, J Electron Mater **29**, 317 (2000).

[13] L.Y. Lee, M. Frentrup, P. Vacek, F.C. Massabuau, M.J. Kappers, D.J. Wallis, and R.A. Oliver, J Cryst Growth **524**, 125167 (2019).

[14] W.D. Nix and B.M. Clemens, J Mater Res **14**, 3467 (1999).

[15] B.W. Sheldon, K.H.A. Lau, and A. Rajamani, J Appl Phys **90**, 5097 (2001).

[16] V. Narayanan, K. Lorenz, W. Kim, and S. Mahajan, Appl Phys Lett **78**, 1544 (2001).

[17] R. Kozak, I. Prieto, Y.A.R. Dasilva, R. Erni, O. Skibitzki, G. Capellini, T. Schroeder, H.V. Känel, and M.D. Rossell, Philos Mag **97**, 2845 (2017).

[18] B.C.D. Cooman and C.B. Carter, Acta Metall **37**, 2765 (1989).

[19] P.M.J. Marée, J.C. Barbour, J.F. Van der Veen, K.L. Kavanagh, C.W.T. Bulle-Lieuwma, and M.P.A. Viegers, J Appl Phys **62**, 4413 (1987).

[20] P.B. Hirsch, Springer Proc Phys **54**, 470 (1991).

[21] L.Y. Lee, M. Frentrup, M.J. Kappers, R.A. Oliver, C.J. Humphreys, and D.J. Wallis, J Appl Phys **124**, 105302 (2018).

[22] D. Nečas and P. Klapetek, Cent Eur J Phys **10**, 181 (2012).

[23] C. Wen, B.H. Ge, Y.X. Cui, F.H. Li, J. Zhu, R. Yu, and Z.Y. Cheng, AIP Adv **4**, 117135 (2014).

[24] M.J. Paisley, Z. Sitar, J.B. Posthill, and R.F. Davis, J Vac Sci Technol A **7**, 701 (1989).

[25] F. Amy and Y.J. Chabal, J Chem Phys **119**, 6201 (2003).

[26] X.H. Wu, D. Kapolnek, E.J. Tarsa, B. Heying, S. Keller, B.P. Keller, U.K. Mishra, S.P. DenBaars, and J.S. Speck, Appl Phys Lett **68**, 1371 (1996).

[27] M. Frentrup, L.Y. Lee, S.-L. Sahonta, M.J. Kappers, F. Massabuau, P. Gupta, R.A. Oliver, C.J. Humphreys, and D.J. Wallis, J Phys D **50**, 433002 (2017).

[28] L.Y. Lee, M. Frentrup, P. Vacek, M.J. Kappers, D.J. Wallis, and R.A. Oliver, J Appl Phys **125**, 105303 (2019).

[29] D. Hull and D.J. Bacon, *Introduction to Dislocations*, 5th ed. (Butterworth-Heinemann, Oxford, 2011).

[30] P.M. Anderson, J.P. Hirth, and J. Lothe, *Theory of Dislocations*, 3rd ed. (Cambridge University Press, Cambridge, 2017).

[31] A.Y.R. Dasilva, R. Kozak, R. Erni, and M.D. Rossell, Ultramicroscopy **176**, 11 (2017).

[32] J.W. Matthews and A.E. Blakeslee, J Cryst Growth **27**, 118 (1974).

[33] A. Fischer, H. Kühne, and H. Richter, Phys Rev Lett **73**, 2712 (1994).

[34] A.F. Wright, J Appl Phys **82**, 5259 (1997).

[35] F. Glas, J Appl Phys **104**, 093520 (2008).